Structural and electrical characterizations of InxGa1-xAs/InP structures for infrared photodetector applications

Tark Asar, Süleyman Özçelik, and Ekmel Özbay

Structural and electrical characterizations of In$_x$Ga$_{1-x}$As/InP structures for infrared photodetector applications

Tarık Asar,[1,2,a)] Süleyman Özçelik,[1,2] and Ekmel Özbay[3,4]

[1]*Department of Physics, Faculty of Science, Gazi University, Ankara 06500, Turkey*
[2]*Photonics Application and Research Center, Gazi University, Ankara 06500, Turkey*
[3]*Nanotechnology Research Center, Bilkent University, Bilkent, Ankara 06800, Turkey*
[4]*Department of Physics, Bilkent University, Bilkent, Ankara 06800, Turkey*

Three InGaAs/InP structures for photodetector applications were grown with different indium compositions by MBE technique. The structural properties of the samples have been obtained by means of high resolution X-ray diffraction and secondary ion mass spectrometry measurements. Three InGaAs/InP metal-semiconductor-metal devices were fabricated at room temperature. The experimental forward and reverse bias current–voltage characteristics of the devices such as ideality factor, barrier height, and saturation current were evaluated considering the structural properties of the grown structures. The carrier recombination lifetime and diffusion length in the devices were also calculated using carrier density and mobility data obtained with Hall effect measurement at room temperature. It was determined that all room temperature fabricated devices improved the Schottky barrier height. Especially, the device fabricated on the lower mismatched structure exhibited barrier height enhancement from 0.2 eV, which is the conventional barrier height to 0.642 eV. In addition, the obtained results show that the room temperature fabricated devices on InGaAs/InP structures can be convenient for infrared photodetector applications. © 2014 AIP Publishing LLC. [http://dx.doi.org/10.1063/1.4868056]

I. INTRODUCTION

III-V compound semiconductor In$_x$Ga$_{1-x}$As ternary alloys have been used in the development of novel optoelectronic device applications such as solar cells,[1–3] photoconductive switches,[4] transistors,[5–7] and photodetectors.[8–13] The InGaAs based semiconductor devices could be fabricated for any wavelength within a spectral range of 0.85–3.60 μm.[8] Especially, the In$_{0.53}$Ga$_{0.47}$As ternary alloy which has a direct band gap with $Eg = 0.75$ eV at room temperature has been grown with lattice matched on InP.[8,14] The InGaAs alloys can be grown on GaAs and InP substrate by epitaxial techniques such as metal organic chemical vapor deposition (MOCVD) and molecular beam epitaxy (MBE).[15–17] Atomic diffusion between the layers and atom exchange at the growing surface during the growth can cause some defects and non-abrupt interfaces.[18,19] Secondary ion mass spectroscopy gives excellent information about the alloy composition, atomic homogeneity, and interface characteristics of grown layers with its depth profile measurements capability in the ppm range.[20–22] As depending on the development of epitaxial growth technology, many semiconductor materials have been developed for improving of infrared devices for sensing or imaging systems. Among these materials, MCT alloys are important due to its narrow band gap. However, the lattice matched substrates with MCT as ZnCdTe are more expensive than III-V substrates and also the growing of MCT structures with low dislocation density on Si or GaAs as alternate substrates have some difficulties.[23] InGaAs along with HgCdTe (MCT) has also been extensively studied

with a great potential for the infrared detector applications[24–32] such as metal-semiconductor-metal (MSM) photodetectors.[33–35] InGaAs detector performance agrees with that of MCT in the 1.5–3.7 μm wavelength range due to similar semiconductor band structures.[36] Nevertheless, InGaAs short wavelength infrared (SWIR) detectors are preferred due to having low dark current and noise and operating at room temperature.[37,38] In addition, InGaAs/InP MSM devices can operate for infrared imaging in the medium wavelength infrared (MWIR) and long wavelength infrared (LWIR) bands at room temperature.[39] In spite of having easy band gap tailoring, well developed theory and experiment, InGaAs detectors which have good materials, dopants, advanced technology, and possible monolithic integration have been preferred.[36] However, the low Φ_B of n-InGaAs, 0.2 eV (Refs. 40–44) leads to quite high leakage currents.[45] Because this low Φ_B of n-InGaAs is not sufficient for quality device applications.[41] There have been extensive studies conducted on its improvement.[46–51] For the enhancement of the barrier height (Φ_B) of n-InGaAs, an important factor is the fabrication conditions of a Schottky contact, as well as the contact material and epilayer crystal quality for the design of 1.55 μm InGaAs/InP MSM photodetectors.[52–54] The previous works on the enhancement of the barrier height have adopted different approaches. One of these uses different metallization temperatures such as low temperature (LT = 77 K) (Ref. 14) and room temperature (RT = 300 K).[40] The other attempts employ a very thin cap layer above InGaAs' active layer, such as InP, GaAs, InAlAs, and AlGaAs as a barrier-enhancement layer,[44,54] or a high-resistivity iron-doped InP layer after the InGaAs absorbing layer,[45] or a thin counter-doped p$^+$-InGaAs surface layer on n-InGaAs,[46–48]

a)trkasar@gazi.edu.tr

or an interfacial oxide-like layer on the n-InGaAs.[49–51] In addition, recently, the effect of low dark current, high responsivity, growth temperature, and anodic oxide passivation layer on the InGaAs/InP photodetectors have been investigated for increasing the infrared photodetector performance.[55–57]

In this present work, the $In_xGa_{1-x}As/InP$ structures for photodetector applications were reported. The three $In_xGa_{1-x}As$ thin film layers were grown on n-type InP substrates by using a solid source MBE system. The structural parameters such as the crystal quality, indium alloy composition (x), lattice parameter (a), grain size (D), dislocation density (δ), and strain (ε) were determined by High resolution X-Ray Diffraction (HRXRD) measurements. Interface abruptness and Indium homogeneity of the grown structures were analyzed by Secondary Ion Mass Spectrometry (SIMS) measurements. The fabrication of three Au/InGaAs/InP/Ni/Au:Ge MSM devices were produced at room temperature. Moreover, the forward and reverse bias experimental I–V measurements of devices were achieved at room temperature. The electrical parameters such as ideality factor (n), barrier height (Φ_B), and saturation current (I_0) were extracted from forward bias I–V characteristics. In addition, carrier lifetime (τ) and diffusion length (L) in fabricated MSM devices were calculated using measured mobility (μ) and carrier density (N) by Hall Effect at room temperature.

II. EXPERIMENTAL

The three n-$In_xGa_{1-x}As$ thin film structures were grown on n-type InP substrates with changing In fraction by using a V80H solid source MBE system. Prior to the growth, InP substrates were chemically cleaned with a novel etching and cleaning process that was prepared by adding an alkaline (sodium hydroxide) solution to the standard acidic cleaning.[58] After loading in the MBE system, the substrate was degassed in a preparation chamber for 1 h at 350 °C in order to remove any residual organics. Then, the substrate was transferred to the deposition chamber and the oxide desorption was observed by RHEED. The n type (Si doped) epitaxial $In_xGa_{1-x}As$ layer with 850 nm thickness at the substrate temperature of 560 °C was grown on three n type InP substrates at different times. The $In_xGa_{1-x}As/InP$ structures were called PD1, PD2, and PD3. To obtain different indium contents in each structure, indium beam equivalent pressure (BEP) was changed while the gallium BEP was kept at a constant value during growth. All of the BEP values and Si cell temperatures are shown in Table I.

HRXRD measurements were carried out on a D-8 Bruker high-resolution diffractometer by using CuKα1 (1.540 Å) radiation, a prodded mirror, and a 4-bounce Ge (220) symmetric monochromator. The angular resolution of the diffractometer was 0.004° with the Si calibration sample.

In order to understand and compare the In composition profile changes after each $In_xGa_{1-x}As/InP$ sample was grown, a SIMS, Hiden system was used for the depth profile of the samples. Information about the In composition and depth profiles of In, Ga, As, P, and Si atoms was obtained. A 5 keV

TABLE I. Si temperatures and BEPs for the $In_xGa_{1-x}As/InP$ structures.

Structure	BEP of Ga (mbar)	BEP of In (mbar)	Temp. of Si Cell (°C)
PD1	3.5×10^{-7}	7.4×10^{-7}	1050
PD2	3.5×10^{-7}	7.5×10^{-7}	1100
PD3	3.5×10^{-7}	7.8×10^{-7}	1100

O_2 gas source was used as a sputtered gun. The sputtering beam was steered over and the analysis signal was taken in an area of 0.5 mm × 0.5 mm at the center of the irradiated spots. The average sputtering rate was kept at 25 nm/min and the sputtered crater depths were determined by a stylus type profilometer (Veeco, Dektak 150).

For the electrical characterizations, all the samples were divided in square parts of 10×10 mm^2 for diode fabrications. The diode fabrication included an ohmic back contact, native oxide removal, and Schottky contact steps. Contacts were obtained by a thermal evaporation system with 1.0×10^{-8} mbar base pressure. First, the samples were cleaned with acetone, methanol, and de-ionized (DI) water, respectively, and dried with nitrogen gas. The ohmic contacts were formed on InP substrates by the deposition of high purity (99.999%) Ni and Au:Ge at room temperature with 200 Å, 2000 Å thicknesses, respectively. Then, the samples were annealed at 360 °C for 3 min under 5.41×10^{-6} mbar vacuum to achieve good ohmic contact behavior. Then, the native oxide on the InGaAs surfaces were removed by $1H_2SO_4$:$1H_2O_2$:$80DI$-H_2O wet chemical etch solution in 1 min. The samples were rinsed in DI-H_2O and dried with nitrogen gas. Finally, dot shaped Schottky contacts with 1200 Å thickness were formed by the deposition of high purity Au (99.999%) at room temperature under 3.73×10^{-6} mbar vacuum. These InGaAs/InP MSM devices were called MSM1 (Au/$In_{0.5410}Ga_{0.4590}As$/InP/Ni/Au:Ge), MSM2 (Au/$In_{0.5430}Ga_{0.4570}As$/InP/Ni/Au:Ge) and MSM3 (Au/$In_{0.5575}Ga_{0.4425}As$/InP/Ni/Au:Ge). Schematic representation of fabricated MSM device and corresponding energy band diagram are given in Figs. 1(a) and 1(b), respectively. In a MSM detector, the IR radiation as depend on Φ_B barrier height is absorbed within the material by interaction with electrons. The detection of the IR light is achieved by measuring electrical output signal produced with changing of the electronic energy distribution in the material. After the fabrication of devices, I–V characteristics were performed using a Keithley 4200 semiconductor parameter analyzer system. In addition, to calculate the carrier lifetime and diffusion length in the MSM devices, mobility and carrier density of the devices were measured by Lake Shore Hall Effect system at room temperature.

III. RESULTS AND DISCUSSION

The indium alloy composition (x) of the grown structures was determined by HRXRD measurements. Fig. 2 shows the recorded ω-2θ X-ray diffraction spectra of the three $In_xGa_{1-x}As/InP$ structures. In the figure, it is clear that the high-intense peaks were derived from InP substrates and the other peaks from $In_xGa_{1-x}As$ layers. The peaks belonged
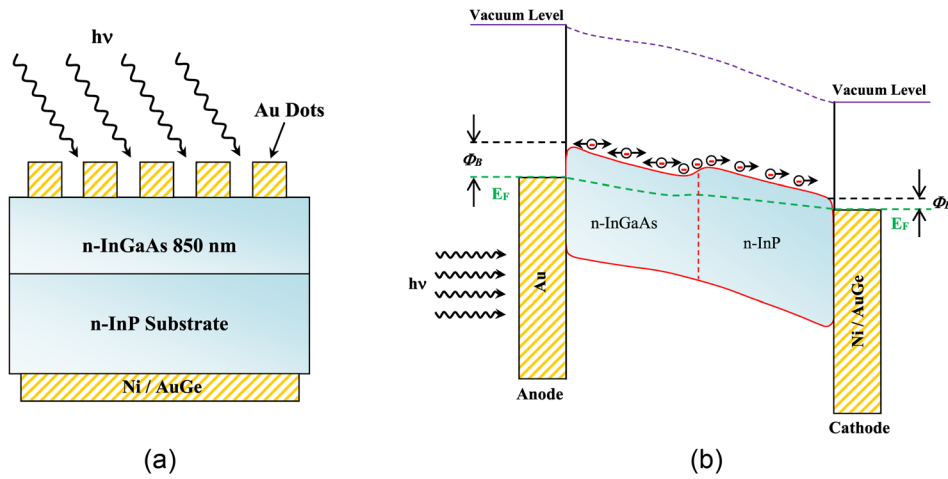
FIG. 1. (a) Schematic representation of the cross section and (b) energy band diagram of the MSM device. Φ_B denotes Schottky barrier height of the device and $\Phi_B{}'$ have to be almost zero for good ohmic contact behavior.

to the In$_x$Ga$_{1-x}$As layers were further separated from the InP substrate peaks due to the increase of the Indium alloy composition in the layer. The peak separation angle can be used to determine the In composition in the alloy. Thus, the x values were found as 54.10%, 54.30%, and 55.75% for PD1, PD2, and PD3 structures, respectively, by using commercial LEPTOS software.[59]

In addition, the full width at half maximum (FWHM) values of XRD peaks for the PD1, PD2, and PD3 structures were determined as 0.014°, 0.020°, and 0.015°, respectively. These values indicate that the grown structures are of good crystal quality. The PD1 structure, which has the lowest FWHM value (0.014°), is the closest one to the lattice-match InGaAs/InP structure.

As seen in Table II, the crystal structural parameters of the three structures such as the lattice parameter (a), grain size (D), dislocation density (δ), and strain (ε) were calculated. They were obtained from the equations given by $a = (\lambda/2\sin\theta).(\sqrt{h^2 + k^2 + l^2})$, $D = (0,9\lambda)/(\beta\cos\theta)$, $\delta = 1/(D^2)$ and $\varepsilon = ((\lambda/D\cos\theta) - \beta).(1/\tan\theta)$, where λ is the X-Ray wavelength, θ is the peak angle value in the ω-2θ scans, hkl are the Miller indices, and β is the FWHM value of the In$_x$Ga$_{1-x}$As peaks.

In Table II, the dislocation density and strain values of the PD1 are lower than the others. The good crystallinity of

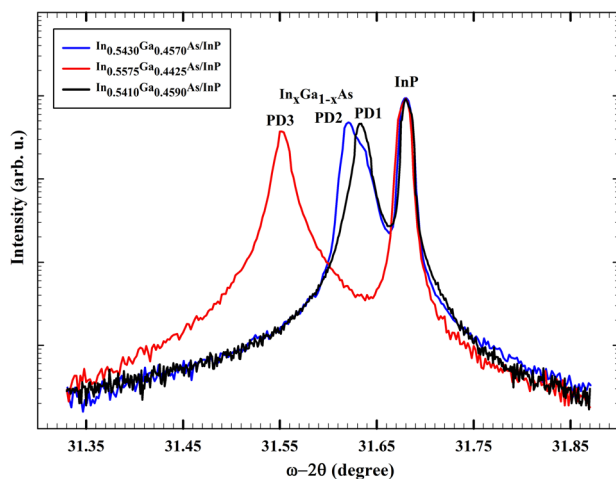the PD1 structure with respect to the other grown structures is also evidenced by these results.

Atomic distributions and interface characteristics of the PD1, PD2, and PD3 structures were analyzed by SIMS depth profile measurements. The SIMS depth profile of the As, Ga, In, and Si atoms in the grown three InGaAs layers on InP are given in Figs. 3–5. It is shown in the SIMS depth profile in the figures that there is no interdiffusion in the layers of all the samples. The samples have excellent abruptness of P distribution on the interface between the layer and substrate and P outdiffussion into the InGaAs layer is a negligible amount. In the interface between the InGaAs layer and InP substrate for all the grown structures, the amount of P is sharply increased while the amount of Ga is sharply decreased. It resulted in the formation of a sharp interface. This result is also an indication of the good quality of the grown InGaAs layer on an InP substrate. In addition, Si doping distribution in the layer has shown similar behavior in all the layers.

As seen in Figure 5, the Ga amounts are approximately the same in the PD1-PD3 structures while the In amounts increased, respectively. These results are in agreement with the Ga and In BEPs, as seen in Table I, indium BEP was increased while the gallium BEP was kept at a constant value for the three structures during the growth. The depth profile analysis of the samples show that In alloy composition (x) was increased with the increasing of In BEP, as expected.

In addition, the homogeneity of the In distribution along the growth direction in the grown layer on InP may be important for device application. As seen in Fig. 6, the In contents have increased along the growth direction for PD2 and PD3 structures. Although the growth temperature is the same for the different structure, this type In content variation can be observed due to the kinetics of the In during epitaxial growth. The variation of the In along the growth direction for the PD2 sample is higher than the PD3. This behavior may cause a shoulder in the HRXRD peak of the InGaAs layer in the PD2 as seen in Fig. 2. The In distribution in the PD1 has good homogeneity with growth direction in the InGaAs layer.

As a result of the analyses of the HRXRD and SIMS measurements, it can be said that factors such as the homogeneity of the In, low dislocation density and strain, sharp

FIG. 2. ω-2θ curves of (004) symmetric planes of the In$_x$Ga$_{1-x}$As/InP structures.

TABLE II. The lattice parameter, grain size, dislocation density, and strain values of the In$_x$Ga$_{1-x}$As/InP structures.

Structure	2θ (deg)	β (deg)	a (Å)	D (nm)	δ ($\times 10^{11}$ cm^{-2})	ε ($\times 10^{-4}$)
PD1	31.633	0.014	11.3047627	589.7777333	0.0028749	0.9583918
PD2	31.621	0.020	11.3089433	412.8321688	0.0058675	1.3696781
PD3	31.551	0.015	11.3333943	550.3477962	0.0033016	1.0296575
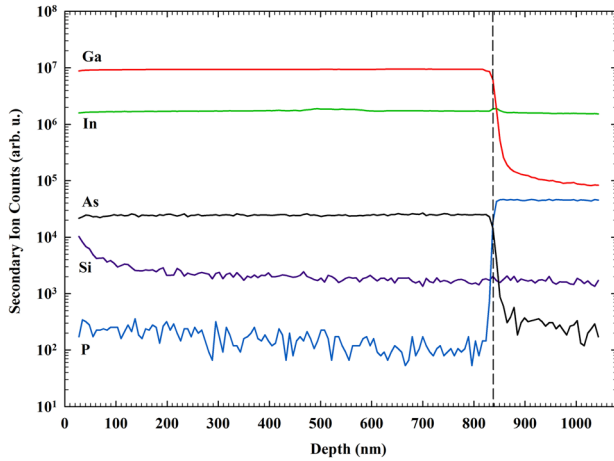
FIG. 3. SIMS profiles of the PD1 (In$_{0.541}$Ga$_{0.459}$As/InP) structure.
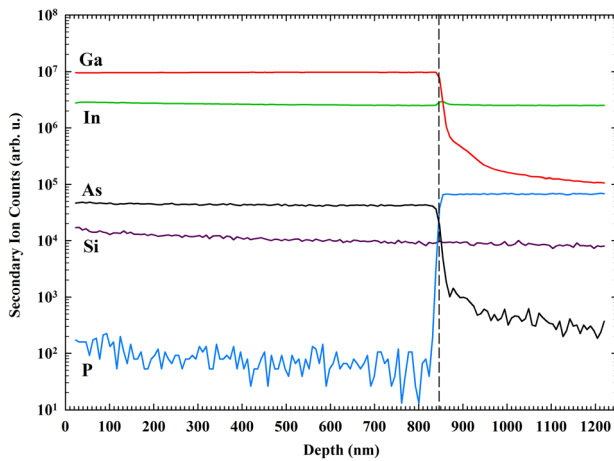
FIG. 4. SIMS profiles of the PD2 (In$_{0.543}$Ga$_{0.457}$As/InP) structure.
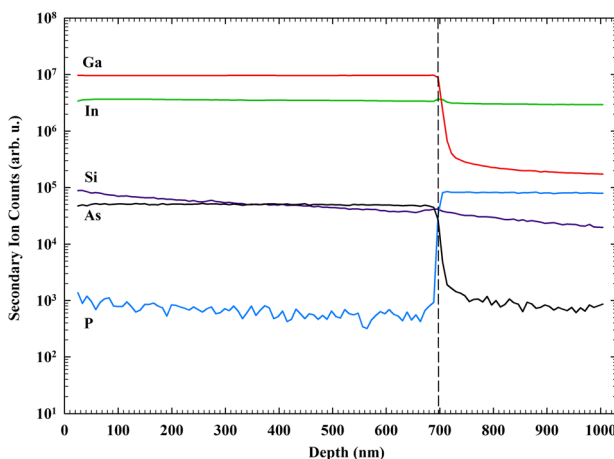
FIG. 5. SIMS profiles of the PD3 (In$_{0.5575}$Ga$_{0.4425}$As/InP) structure.

interface of the layer/substrate and FWHM of the HRXRD peak have significant effects on the growth of the In$_{0.543}$Ga$_{0.457}$As/InP structure, which is the one that fits best to the lattice matched In$_{0.53}$Ga$_{0.47}$As/InP structure.

The forward and reverse-bias $I-V$ characteristics of InGaAs/InP MSM devices were measured to investigate certain electrical properties of structures such as the ideality factor (n), barrier height (Φ_B), and saturation current (I_0). Fig. 7 shows the semi-logarithmic $I-V$ characteristics of the MSM1, MSM2, and MSM3 structures at room temperature. According to the thermionic emission theory, the relationship between the applied forward voltage ($V \geq kT/q$) and the current can be expressed as shown below[60]

$$I = I_o\left[\exp\left(\frac{q(V - IR_s)}{nkT}\right) - 1\right],\tag{1}$$

where V is the forward bias voltage, n the ideality factor, k is the Boltzmann constant, T is the temperature in K, and the term IR_s is the voltage drop across the series resistance of the device. The voltage $V_d = V - IR_s$ across the diode can be expressed in terms of the total voltage drop V across the series combination of the device and the series resistance.

In Fig. 7, the saturation current I_0 is derived from the straight-line intercept of ln$I$ at zero bias and is

$$I_0 = AA^*T^2\exp\left(-\frac{q\Phi_B}{kT}\right),\tag{2}$$

where A, A^*, q, and Φ_B are the diode area, the effective Richardson constant (for n-type InP 9.4 A cm^{-2} K^{-2}),[61] the electronic charge, and the zero-bias barrier height, respectively. From Eq. (1), the ideality factor can be written as
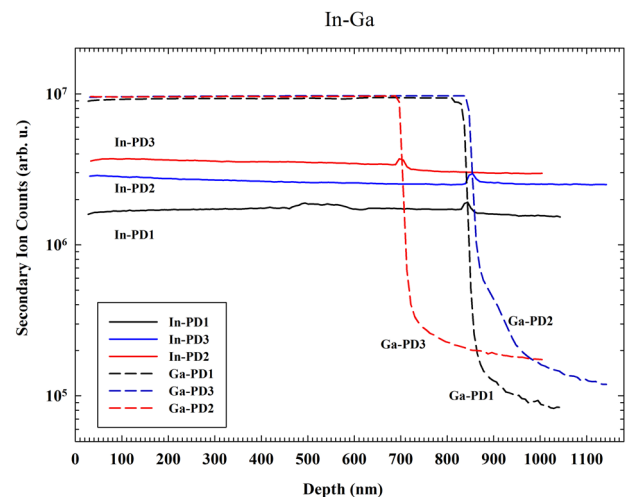

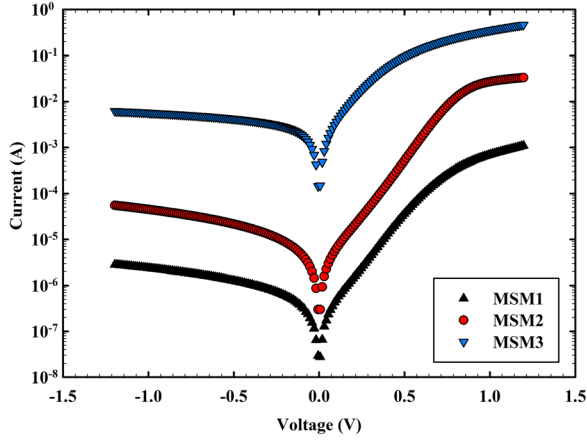FIG. 6. In and Ga SIMS profiles of the structures.

FIG. 7. The semi-logarithmic forward and reverse bias current-voltage characteristics of the MSM devices at room temperature.

$$n = \frac{q}{kT}\frac{dV}{d\ln(I)}, \tag{3}$$

n is used to calculate the deviation from the ideal thermionic model. Φ_B was calculated using the theoretical value of A^* and extrapolated I_0 at room temperature according to

$$\Phi_B = \frac{kT}{q}\ln\left(\frac{AA^*T^2}{I_0}\right). \tag{4}$$

The calculated values of n and Φ_B obtained from Eqs. (3) and (4) are shown in Table III.

As seen from the Table III, the Φ_B values were calculated as 0.642 eV for MSM1, 0.582 eV for MSM2 and 0.382 eV for MSM3. These values correspond the wavelengths of 1.931 μm, 2.130 μm, and 3.246 μm and they can be deemed suitable for infrared photodetector applications. This study has achieved the same result with the above-mentioned literature, which has used fabrication processes such as low temperature fabrication and additional layer growth in the structure, by only fabricating diodes at room temperature. The enhancement of the Schottky barrier height with this study can be attributed to the crystal quality of the structure.

In addition, the performance of optoelectronic devices include InGaAs/InP infrared photodetector is critically dependent on some important parameters such as mobility, carrier density, recombination lifetime, and diffusion length.[62] Recombination lifetime (τ) and diffusion length (L) for InGaAs/InP MSM devices were calculated with obtained the carrier density (N) and mobility (μ) data by Hall Effect measurements at room temperature.

The total recombination lifetime is given by[63]

$$\frac{1}{\tau} = \frac{1}{\tau_{SRH}} + \frac{1}{\tau_R} + \frac{1}{\tau_A}. \tag{5}$$

TABLE III. Electrical parameters for the InGaAs/InP MSM devices.

Device	n	Φ_B (eV)	Io (A)
MSM1	3.59	0.642	1.78×10^{-7}
MSM2	3.76	0.582	1.97×10^{-6}
MSM3	4.07	0.382	1.46×10^{-3}

TABLE IV. Carrier density, mobility, diffusion coefficient, carrier lifetime, and diffusion length of the MSM devices.

Device	T (K)	N (1/cm³)	μ (cm²/V.s)	D (cm²/s)	τ (ns)	L (μm)
MSM1	299.839	3.818×10^{17}	4553.1	116.519	20.040	15.281
MSM2	296.972	3.490×10^{17}	3563.3	92.069	18.314	12.985
MSM3	296.336	3.891×10^{17}	3659.6	93.453	17.973	12.960

In terms of doping concentrations N, the Eq. (5) can be rewritten as

$$\tau = \left[\tau_{SRH}^{-1} + BN + CN^2\right]^{-1}. \tag{6}$$

As seen from the equations, the total recombination lifetime depends upon the N separate into the three parts as Shockley–Read–Hall (SRH), Auger and radiative recombination. From 10^{16} to 10^{18} cm^{-3} doping range, radiative recombination is dominant and the total lifetime varies as $1/N$.[64] Then, the total lifetime can be given by

$$\tau = [BN]^{-1}. \tag{7}$$

Here, the radiative recombination coefficient B is 2×10^{-11} cm^{-3} s^{-1} for InP and 1.43×10^{-10} cm^{-3} s^{-1} for InGaAs.[25,64]

The diffusion length (L) can be calculated by Eq. (8). L leads the distribution of carrier in devices depend on minority carrier injection and diffusion.

The diffusion length can be derived from the carrier lifetime τ by

$$L_{n,p} = \sqrt{\tau . D_{n,p}}, \tag{8}$$

where the diffusion coefficient $D_{n,p}$ is given by the Einstein relation,

$$D_{n,p} = \mu_{n,p}\frac{kT}{q}. \tag{9}$$

Here, $\mu_{n,p}$ is the carrier mobility, k is the Boltzmann's constant, and q is the electrical charge on electron.[65]

Consequent of the theoretical modelling, as seen the Table IV, the carrier lifetime and diffusion length can be derived from the mobility and carrier density, which were obtained from the Hall measurements at room temperature.

IV. CONCLUSIONS

We have presented experimental and theoretical evidences that the room temperature metallization process in this work can be used for InGaAs/InP MSM photodetector by engineering the Schottky barrier height. For this purpose, the indium alloy composition (x) and room temperature metallization effect have been investigated on the structural and electrical properties of MBE grown InGaAs/InP structures. Structural parameters such as alloy composition, lattice parameter, grain size, dislocation density, and strain of the structures have been obtained by HRXRD measurements.

Indium homogeneity and abruptness in the interface of the grown $In_xGa_{1-x}As$ layers on InP substrates are identified by SIMS depth profile measurements. It was seen that there was a good agreement between the change of the x values obtained from the HRXRD and SIMS measurements. In the SIMS measurements, the great steepness of As and P distributions across the interface between InGaAs and InP was obtained in all the structures. Important device parameters such as ideality factor, Schottky barrier height and saturation current of room temperature fabricated MSM devices were obtained by current-voltage measurements. In addition, the carrier lifetime and diffusion length in the MSM devices were calculated using the mobility and carrier density data obtained from Hall Effect measurements. The values of Φ_B were calculated 0.642 eV for MSM1, 0.582 eV for MSM2, and 0.382 eV for MSM3 from room temperature forward-bias I-V measurements. It was seen that the Schottky barrier height Φ_B was increased from the conventional barrier height 0.2 eV to 0.642 eV. These results show that an important improvement of the barrier height is obtained by the fabrication of the diode at room temperature process. Improvement on the barrier height of MSM devices can be attributed to the bigger grain size, lower FWHM, lower dislocation density, lower strain, and great steepness of As and P distributions of the grown samples. Besides these parameters, Indium homogeneity in the epilayer may affect the electrical parameters of the devices. In addition, it can be said that these types of structures can be more convenient for photodetector applications especially due to fabricating at room temperature.

ACKNOWLEDGMENTS

[1]T. Asar, B. Sarıkavak, M. K. Öztürk, T. Mammadov, and S. Özçelik, "Effects of annealing on the structural properties of GaAs-based quantum well solar cells," J. Opt. Adv. Mater. **11**(11), 1627–1631 (2009).

[2]T. E. Tzeng, K. Y. Chuang, T .S. Lay, and C. H. Chang, "Broadband InGaAs quantum dot-in-a-well solar cells of p-type wells," J. Cryst. Growth **378**, 583–586 (2013).

[3]S. Turner, S. Mokkapati, G. Jolley, L. Fu, H. H. Tan, and C. Jagadish, "Periodic dielectric structures for light-trapping in InGaAs/GaAs quantum well solar cells," Opt. Exp. **21**(S3), A324–A335 (2013).

[4]B. Heshmat, H. Pahlevaninezhad, and T. E. Darcie, "Optical efficiency enhancement methods for terahertz receiving photoconductive switches," Opt. Laser Technol. **54**, 297–302 (2013).

[5]Parveen, M. Gupta, R. S. Gupta, and J. Jogi, "RF characterization of 100-nm separate gate InALAs/InGaAs DG-HEMT," Microwave Opt. Technol. Lett. **55**(11), 2796–2803 (2013).

[6]S. Hung, Q. Luan, H. Lin, S. Li, and S. Chang, "Embedded-Ge source and drain in InGaAs/GaAs dual channel MESFET," Curr. Appl. Phys. **13**, 1577–1580 (2013).

[7]T. Teng, A. Xu, L. Ai, H. Sun, and M. Qi, "InP/InGaAs/InP DHBT structures with high carbon-doped base grown by gas source molecular beam epitaxy," J. Cryst. Growth **378**, 618–621 (2013).

[8]J. Kaniewski and J. Piotrowski, "InGaAs for infrared photodetectors," Phys. Technol., Opto-electron. Rev. **12**(1), 139–148 (2004).

[9]C. L. Tsai, K. Y. Cheng, S. T. Chou, and S. Y. Lin, "InGaAs quantum wire infrared photodetector," Appl. Phys. Lett. **91**, 181105 (2007).

[10]S. Ozer, U. Tumkaya, and C. Besikci, "Large format AlInAs–InGaAs quantum-well infrared photodetector focal plane array for midwavelength infrared thermal imaging," IEEE Photon. Technol. Lett. **19**(18), 1371–1373 (2007).

[11]J. Piotrowski and J. Kaniewski, "Optimisation of InGaAs infrared photovoltaic detectors," IEE Proc.-Optoelectron. **146**(4), 173–176 (1999).

[12]J. Piotrowski, J. Kaniewski, and K. Reginski, "Modeling and optimization of InGaAs infrared photovoltaic detectors," Nucl. Instrum. Methods Phys. Res. A **439**, 647–650 (2000).

[13]J. Yuan, B. Chen, and A. L. Holmes, "Near-infrared quantum efficiency of uncooled photodetectors based on InGaAs/ GaAsSb quantum wells lattice-matched to InP," Electron. Lett. **47**(20), 1144–1145 (2011).

[14]H. J. Lee, W. A. Anderson, H. Hardtdegen, and H. Lüth, "Barrier height enhancement of Schottky diodes on n-$In_{0.53}Ga_{0.47}As$ by cryogenic processing," Appl. Phys. Lett. **63**, 1939–1941 (1993).

[15]J. Schleeh, H. Rodilla, N. Wadefalk, P.Å. Nilsson, and J. Grahn, "Cryogenic noise performance of InGaAs/InAlAs HEMTs grown on InP and GaAs substrate," Solid-State Electron. **91**, 74–77 (2014).

[16]Y. Yasuda, S. Koh, K. Ikeda, and H. Kawaguchi, "Crystal growth of InGaAs/InAlAs quantum wells on InP(110) by MBE," J. Cryst. Growth **364**, 95–100 (2013).

[17]A. Jasik, A. Wnuk, A. Wojcik-Jedlinska, R. Jakiela, J. Muszalski, W. Strupinski, and M. Bugajski, "The influence of the growth temperature and interruption time on the crystal quality of InGaAs/GaAs QW structures grown by MBE and MOCVD methods," J. Cryst. Growth **310**, 2785–2792 (2008).

[18]Z. LilientalWeber, Y. Chen, P. Werner, N. Zakharov, W. Swider, J. Washburn, J. F. Klem, and J. Y. Tsao, "Interfacial defects and morphology of InGaAs epitaxial layers grown on tilted GaAs substrates," J. Vac. Sci. Technol. B **11**, 1379–1383 (1993).

[19]Y. Fujiwara, Y. Nonogaki, R. Oga, A. Koizumi, and Y. Takeda, "Reactor structure dependence of interface abruptness in GaInAs/InP and GaInP/GaAs grown by organometallic vapor phase epitaxy," Appl. Surf. Sci. **216**, 564–568 (2003).

[20]Y.-P. An, H. Yang, T. Mei, Y.-D. Wang, J.-H. Teng, and C.-D. Xu, "Cap layer influence on impurity-free vacancy disordering of InGaAs/InP quantum well structure," Chin. Phys. Lett. **27**(1), 017302 (2010).

[21]B. R. Chakraborty, "Characterization of interfaces in nanoscale semiconductor devices by optimization of depth resolution in SIMS depth profiling," Appl. Surf. Sci. **221**, 143–154 (2004).

[22]K. Kadoiwa, K. Ono, and Y. Ohkura, "Zn diffusion behavior at the InGaAsP/InP heterointerface grown using MOCVD," J. Cryst. Growth **297**, 44–51 (2006).

[23]A. J. Stoltz, J. D. Benson, R. Jacobs, P. Smith, L. A. Almeida, M. Carmody, S. Farrell, P. S. Wijewarnasuriya, G. Brill, and Y. Chen, "Reduction of dislocation density by producing novel structures," J. Electron. Mater. **41**, 2949 (2012).

[24]A. Baliga, D. Trivedi, and N. Anderson, "Tensile-strain effects in quantum-well and superlattice band structures," Phys. Rev. B **49**, 10402–10416 (1994).

[25]X. D. Wang, W. D. Hu, X. S. Chen, W. Lu, H. J. Tang, T. Li, and H. M. Gong, "Dark current simulation of InP/$In_{0.53}Ga_{0.47}As$/InP p-i-n photodiode," Opt. Quantum Electron. **40**, 1261–1266 (2008).

[26]X. Ji, B. Liu, Y. Xu, H. Tang, X. Li, H. M. Gong, B. Shen, X. Yang, P. Han, and F. Yan, "Deep-level traps induced dark currents in extended wavelength $In_xGa_{1-x}As$/InP photodetector," J. Appl. Phys. **114**, 224502 (2013).

[27]X. M. Zhang, C. Liang, G. Liu, D. Y. Fan, P. Lang, Z. B. Sun, H. Q. Ma, R. Zhang, and M. Lei, "Analysis of a InGaAs/InP single photon detector at 1550 nm," J. Mod. Opt. **60**(12), 983–986 (2013).

[28]A. Tosi, C. Scarcella, G. Boso, and F. Acerbi, "Gate-free InGaAs/InP single-photon detector working at up to 100 Mcount/s," IEEE Photon. J. **5**(4), 6801308 (2013).

[29]A. McCarthy, X. Ren, A. D. Frera, N. R. Gemmell, N. J. Krichel, C. Scarcella, A. Ruggeri, A. Tosi, and G. S. Buller, "Kilometer-range depth imaging at 1550 nm wavelength using an InGaAs/InP single-photon avalanche diode detector," Opt. Exp. **21**(19), 22098–22113 (2013).

[30]G. A. Umana-Membreno, H. Kala, J. Antoszewski, Z. H. Ye, W. D. Hu, R. J. Ding, X. S. Chen, W. Lu, L. He, J. M. Dell, and L. Faraone, "Depth profiling of electronic transport parameters in n-on-p boron-ion-implanted vacancy-doped HgCdTe," J. Electron. Mater. **42**(11), 3108–3113 (2013).

[31]J. Zhang, G. K. O. Tsen, J. Antoszewski, J. M. Dell, L. Faraone, and W. D. Hu, "A study of sidewall effects in HgCdTe photoconductors passivated with MBE-grown CdTe," J. Electron. Mater. **39**(7), 1019–1022 (2010).

[32]A. Rogalski, J. Antoszewski, and L. Faraone, "Third-generation infrared photodetector arrays," J. Appl. Phys. **105**, 091101 (2009).

[33]R. Chen, J. Fu, D. A. B. Miller, and J. S. Harris, "Spectral shaping of electrically controlled MSM-based tunable photodetectors," IEEE Photon. Technol. Lett. **17**(10), 2158–2160 (2005).

[34]K. C. Song, M. A. Matin, B. Robinson, J. G. Simmons, D. A. Thompson, and P. Mascher, "High performance InP/InGaAs-based MSM photodetector operating at 1.3-1.5 μm," Solid State Electron. **39**(9), 1283–1287 (1996).

[35]N. Debbar, A. Rudra, J.-F. Carlin, and M. Ilegems, "High-speed InP/GaInAs metal-semiconductor-metal photodetectors grown by chemical beam epitaxy," Appl. Phys. Lett. **65**(2), 228–230 (1994).

[36]A. Rogalski, "Infrared detectors: status and trends," Progr. Quantum Electron. **27**, 59–210 (2003).

[37]N. K. Dhar, R. Dat, and A. K. Sood, "Advances in infrared detector array technology," in *Optoelectronics – Advanced Materials and Devices*, edited by S. L. Pyshkin and J. M. Ballato (InTech, 2013), Chap. 7.

[38]C. D. Tran, "Infrared multispectral imaging: principles and instrumentation," Appl. Spectrosc. Rev. **38**(2), 133–153 (2003).

[39]H. Kazemi, K. Shinohara, G. Nagy, W. Ha, B. Lail, E. Grossman, G. Zummo, W. R. Folks, J. Alda, and G. Boreman, "First THz and IR characterization of nanometer-scaled antenna-coupled InGaAs/InP Schottky-diode detectors for room temperature infrared imaging," Proc. SPIE **6542**, 65421J (2007).

[40]L. He, M. J. Costello, K. Y. Cheng, and D. E. Wohlert, "Enhanced Schottky barrier on InGaAs for high performance photodetector application," J. Vac. Sci. Technol. A **16**(3), 1646–1649 (1998).

[41]P. Kordoš, M. Marso, R. Meyer, and H. Lüth, "Schottky barrier height enhancement on n-In$_{0.53}$Ga$_{0.47}$As," J. Appl. Phys. **72**, 2347–2355 (1992).

[42]K. Kajiyama, Y. Mizushima, and S. Sakata, "Schottky barrier height of n-In$_x$Ga$_{1-x}$As diodes," Appl. Phys. Lett. **23**, 458 (1973).

[43]H. Tamura, A. Yoshida, S. Muto, S. Muto, and S. Hasuo, "Schottky barrier height of Al/n-In$_{0.53}$Ga$_{0.47}$As diodes," Jpn. J. Appl. Phys. Part 2 **26**, L7 (1987).

[44]U. Kunze and W. Kowalsky, "Characterization of Schottky barrier diodes by means of modulation technique," J. Appl. Phys. **63**, 1597 (1988).

[45]L. Malacky, R. Klockenbrink, J. Darmo, H.-H. Wehmann, G. Zwinge, and A. Schlachetzki, "InGaAs Schottky contacts with an iron-doped InP enhancement layer," J. Phys. D: Appl. Phys. **27**, 2414–2417 (1994).

[46]T. Kikuchi, H. Ohno, and H. Hasegawa, "Ga$_{0.47}$In$_{0.53}$As metal-semiconductor-metal photodiodes using a lattice mismatched Al$_{0.4}$Ga$_{0.6}$As Schottky assist layer," Electron. Lett. **24**(19), 1208–1210 (1988).

[47]J. H. Kim, S. S. Li, L. Figueroa, T. F. Carruthers, and R. S. Wagner, "A high-speed InP-based In$_x$Ga$_{1-x}$As Schottky barrier infrared photodiode for fiber-optic communications," J. Appl. Phys. **64**, 6536 (1988).

[48]W. P. Hong, G. K. Chang, and R. Bhat, "High-performance Al$_{0.15}$Ga$_{0.85}$As/In$_{0.53}$Ga$_{0.47}$As MSM photodetectors grown by OM-CVD," IEEE Trans. Electron Devices **36**(ED), 659–662 (1989).

[49]J. B. D. Soole, H. Schumacher, H. P. LeBlanc, R. Bhat, and M. A. Koza, "High-frequency performance of InGaAs metal-semiconductor-metal photodetectors at 1.55 and 1.3 μm wavelengths," Appl. Phys. Lett. **55**, 729–731 (1989).

[50]K. C. Hwang, S. S. Li, C. Park, and T. J. Anderson, "Schottky barrier height enhancement of n-In$_{0.53}$Ga$_{0.47}$As by a novel chemical passivation technique," J. Appl. Phys. **67**, 6571 (1990).

[51]D. Kuhl, F. Hieronymi, E. M. Böttcher, T. Wolf, A. Krost, and D. Bimberg, "Very high-speed metal-semiconductor-metal InGaAs:Fe photodetectors with InP:Fe barrier enhancement layer grown by metalorganic chemical vapour deposition," Electron. Lett. **26**, 2107 (1990).

[52]E. Rusu, E. Budianu, S. Nan, and M. Purica, "Schottky barrier on the InGaAs/InP heterostructures grown by the CL-VPE tecnique for photodetectors," in *IEEE 19th International Semiconductor Conference* (1996), pp. 211–214.

[53]A. F. Salem, A. W. Smith, and K. F. Brennan, "Heterostructure on theoretical study of the effect of an AlGaAs double metal-semiconductor-metal photodetector performance," IEEE Trans. Electron Devices **41**(7), 1112–1119 (1994).

[54]St. Kollakowski, U. Schade, E. H. Böttcher, D. Kuhl, D. Bimberg, P. Ambree, and K. Wandel, "Silicon dioxide passivation of InP/InGaAs metal-semiconductor-metal photodetectors," J. Vac. Sci. Technol. B **14**, 1712–1718 (1996).

[55]B. Li, H. W. Yang, Q. Gui, X. H. Yang, J. Wang, X. P. Wang, S. Q. Liu, and Q. Han, "Ultra low dark current, high responsivity and thin multiplication region in InGaAs/InP avalanche photodiodes," Chin. Phys. Lett. **29**(11), 118503 (2012).

[56]Y. Gu, Y. G. Zhang, K. Wang, X. Fang, C. Li, L. Zhou, A. Z. Li, and H. Li, "Effects of growth temperature and buffer scheme on characteristics of inp-based metamorphic ingaas photodetectors," J. Cryst. Growth **378**, 65–68 (2013).

[57]A. Rouvie, O. Huet, S. Hamard, J. P. Truffer, M. Pozzi, J. Docebert, E. Costard, M. Zecri, P. Maillart, Y. Reibel, and A. Pecheur, "SWIR InGaAs focal plane arrays in France," in *Proceedings of SPIE 8704, Infrared Technology and Applications XXXIX* (2013), p. 870403.

[58]J. Liu, Y. Zhao, Z. Dong, F. Yang, F. Wang, K. Cao, T. Liu, H. Xie, and T. Chen, "Improvement of the surface quality of semi-insulating InP substrates through a novel etching and cleaning method," J. Vac. Sci. Technol. A **31**, 031404 (2013).

[59]LEPTOS, *User Manual Version 2* (2004), www.bruker-axs.de.

[60]E. H. Rhoderick and R. H. Williams, *Metal-Semiconductor Contacts* (Clarendon, Oxford, 1988).

[61]H. Hbib, O. Bonnaud, and B. Fortin, "Electrical characteristics of (n)-InP MIS diodes with a PO$_x$N$_y$ interfacial layer deposited at low temperature," Semicond. Sci. Technol. **12**, 609–613 (1997).

[62]W. K. Metzger, M. W. Wanlass, R. J. Ellingson, R. K. Ahrenkiel, and J. J. Carapella, "Auger recombination in low-band-gap," Appl. Phys. Lett. **79**(20), 3272–3274 (2001).

[63]R. K. Ahrenkiel, R. Ellingson, S. Johnston, and M. Wanlass, "Recombination lifetime of In$_{0.53}$Ga$_{0.47}$As as a function of doping density," Appl. Phys. Lett. **72**(26), 3470–3472 (1998).

[64]Y. Lv, N. Wang, C. Zhuang, P. Li, B. Han, and H. Gong, "The uniformity of InGaAs in InP/InGaAs/InP by microwave photoconductivity decay (μ-PCD) carrier lifetime measurement," Semicond. Sci. Technol. **21**, 771–774 (2006).

[65]E. Kuphal, K. Mause, K. Miethe, A. Eisenbach, F. Fielder, and A.Corbet, "Electron diffusion length in InGaAs:Zn derived from heterostructure bipolar transistors," Solid-State Electron. **38**(4), 795–799 (1995).